Determination of the thermal conductivity of opalinus clay via simulations of experiments performed at the Mont Terri underground laboratory

C. Mügler [a,*], M. Filippi [b], Ph. Montarnal [b], J.-M. Martinez [b], Y. Wileveau [c]

[a]CEA, DSM/LSCE, Centre de Saclay, Bât. 701, 91191 Gif-sur-Yvette Cedex, France
[b]CEA, DEN/DM2S, Centre de Saclay, Bât. 454, 91191 Gif-sur-Yvette Cedex, France
[c]ANDRA, Laboratoire de Meuse/Haute-Marne, BP 3, 55290 Bure, France

Abstract

Storage in deep geological formations is a potential solution for the management of high-level radioactive wastes. In this context, different types of rocks such as argillite are extensively studied. In the Mont Terri underground laboratory (Switzerland), several experiments have been performed in order to characterize the properties of the opalinus clay. One of these experiments, called HE-C, has consisted in measuring in situ the time evolution of the rock temperature submitted to a heating source. Experimental measurements have shown that the thermal behaviour of the clay was not homogeneous around the borehole where the heater was installed. Furthermore, 3D direct numerical simulations of this experiment performed with the code Cast3M have proved that it was necessary to introduce a new parameter α to model the amount of electric power lost in cables and by air convection inside the metallic tube containing the heater. A numerical simulation–optimization technique has been used to estimate the thermal longitudinal and transverse conductivities ($\lambda_{//}$ and $\lambda_{\perp}$) of the host rock. It consists in minimizing an objective function that is the sum of the squared differences between measured and calculated temperatures. But this method induced a lot of Cast3M simulations. In order to drastically reduce the CPU time, we used a neural network approximation built from a sample training of 1100 Cast3M simulations. It allowed us to calculate the objective function for 500 000 different values of the triplet ($\lambda_{//}, \lambda_{\perp}, \alpha$).

Finally, we obtained the following values for the thermal conductivities

– on one side of the borehole, $\lambda_{//} = 1.84 \pm 0.04$ W m^{-1} K^{-1} and $\lambda_{\perp} = 0.55 \pm 0.03$ W m^{-1} K^{-1};
– on the other side, $\lambda_{//} = 1.90 \pm 0.07$ W m^{-1} K^{-1} and $\lambda_{\perp} = 1.07 \pm 0.09$ W m^{-1} K^{-1}.

* Corresponding author. Fax: +33 1 69 08 77 16.
  E-mail address: claude.mugler@cea.fr (C. Mügler).

The estimated thermal conductivities $\lambda_\perp$ perpendicular to the bedding plane are quite different. It is perhaps caused by the presence of an intensive fractured zone on one side of the borehole, due to bentonite swelling. It can also be due to the presence of a bed of carbonated rock.

1. Introduction

Disposal in deep geological formations is a potential solution for the management of spent fuel and high-level radioactive wastes. Concepts of nuclear waste storage in deep geological formations are all based on a multibarrier system composed of engineered and natural barriers. The engineered barriers are composed of vitrified, cemented or bituminized nuclear wastes encapsulated in a canister, metal overpack and buffer material such as clay engineered barrier. The geologic formation constitutes the ultimate barrier. In the near-field of a high-level radioactive waste repository, coupled thermo–hydro–mechanical and chemical (T–H–M–C) processes will occur, involving processes such as heat generation and transport (due to radioactive decay of nuclear waste), infiltration of groundwater (hydrological processes), swelling pressure of buffer material due to saturation (mechanical processes) and chemical evolution of buffer material and porewater (chemical processes). The safety assessment of nuclear waste disposals needs to predict the migration of radionuclides and chemical species through the engineered barriers and through the geological medium. It is therefore necessary to characterize thermal and hydraulic properties of the geological medium but also its ability to retain and delay the radionuclide migration. It is with this aim in view that different types of rocks such as argillite are extensively studied (Lalieux et al., 1996). Argillaceous formations are of particular interest because their very low permeability and their strong capacity for radionuclide retention give them good confining properties. The French Agency for the Management of Radioactive Waste (ANDRA) has selected an argillaceous site located in the East of France (Meuse/Haute-Marne) where it will develop an experimental research program focusing on the characterization of confinement properties of argillite and on the study of their potential modification submitted to disturbances associated to the construction and working of a geological waste disposal. More information can be obtained from internal reports (Andra, 2003) and on the website (http://www.andra.fr). As this French underground research laboratory is not yet available, preliminary experiments are performed in the Mont Terri underground laboratory in north-western Switzerland. This laboratory is situated in an opalinus clay geological sediment formation. The formation is named after the ammonite *Leioceras Opalinum*, a mollusc fossil of the Mesozoic period that is present in large numbers in it. The Mont Terri project is an international research project under the patronage of the Swiss National Hydrological and Geological Survey. Several organisations are partners in the project, such as ANDRA and IRSN (France), BGR (Germany), ENRESA (Spain), Nagra (Switzerland), JNC and Obayashi (Japan) and SCKCEN (Belgium). All these organisations are involved in the management of nuclear radioactive wastes and their potential storage in geological formations. The aims of the project are to analyse the hydrogeological, geochemical and rock mechanical properties of an argillaceous formation, the changes of these properties induced by the excavation of galleries and to evaluate and improve appropriate investigation techniques (Thury and Bossart, 1999; Gautschi, 2001; Bossart et al., 2002; Croisé et al., 2004). The aim of one of the experiments performed by ANDRA in the Mont Terri underground laboratory is to characterize the opalinus clay thermal properties. Indeed, spent fuel from reactors and high-level waste are heat-generating. So, they are held in interim storage for several decades to allow this radiogenic heat to decay to acceptable levels. Such wastes will be emplaced in a repository only when the rock in the disposal zone will not be heated to unacceptable high temperatures. At the planned depth for a repository (about 500 m), the rock has a temperature of 30 to 40 °C (Nagra, 2002). Then, the question is whether or not the rock is altered when it is

heated to a temperature of about 100 °C. Thermal effects in rock materials have relatively long time and spatial scales, of the order of the metre and the year, respectively. So, thermal measurements on small rock samples performed in laboratory are not sufficient. In situ experiments are required to study the scale dependence of the rock thermal properties. Thermal in situ experiments have already been performed in granitic rocks and in volcanic tuffs, in an international cooperative project named DECOVALEX (acronym for Development of Coupled thermo–hydro–mechanical (THM) models and their VALidation against Experiments). This project was established in 1992 by national regulatory authorities and waste management organisations involved in nuclear waste disposal (Stephansson et al., 1996). Several papers in the GeoProc (2003) conference proceedings are dedicated to the DECOVALEX project (GeoProc, 2003). In particular, in the third phase of the project, named DECOVALEX III, starting in 1999 and ending in 2003, the FEBEX experiment (acronym for Full-scale Engineered Barriers EXperiments in crystalline host rock) was a full-scale in situ experiment performed on a heater–buffer–rock system in the Grimsel Test Site in Switzerland, with a long period of heating followed by cooling. The aim of FEBEX was to demonstrate the present capabilities for building bentonite barriers in conditions similar to actual repository design and providing monitoring data to understand and model coupled THMC processes in the near field. The second task of DECOVALEX III, the Drift Scale Test (DST) in the Exploratory Studies Facility (ESF) at Yucca Mountain, was also a large-scale thermal test conducted by the U.S. Department of Energy to evaluate the suitability of the Yucca Mountain site for a potential nuclear waste repository. These in situ thermal experiments were modelled and simulated by several research teams and agreement in temperature was good.

Thermal in situ experiments performed in the Mont Terri underground laboratory are quite similar to some experiments of the DECOVALEX project but the rock in which they are performed is very different: fractured granitic rocks or volcanic tuffs in the DECO-VALEX project, opalinus clay in the Mont Terri project. The purpose of the experiments presented and simulated in this paper is to identify thermal conductivity coefficients of the opalinus clay in

order to model heat transfer in such an argillite. Experiments consist in measuring in situ clay temperature variation when submitted to a heating source. Experimental conditions will be described in Section 2 of this paper. Afterwards, Section 3 will give a description of the modelling and numerical methods used to perform direct numerical simulations of the experiments. Numerical simulations are performed with the Cast3M code and a numerical simulation–optimization technique is used to determine the thermal conductivity of the opalinus clay. The optimization technique using a neural network will be presented in Section 4. In Section 5, experimental measurements and numerical results will be compared and finally, values for the thermal conductivity will be proposed.

2. Description of experiment

The main objective of the in situ experiment presented in this paper is to characterize the thermal properties of the opalinus clay.

The experiment was set up in a gallery of the Mont Terri underground laboratory in 2002.

2.1. The opalinus clay formation at Mont Terri

The opalinus clay geological sediment layer investigated in the Mont Terri rock laboratory was formed some 180 million years ago during the Jurassic period (Dogger, Aalenian) as a marine sediment made up of fine mud particles (see Fig. 1). The weight of the more recent sediments deposited on top of the opalinus clay had the effect of squeezing water out of the rock. So, it gradually became an indurated claystone. The opalinus clay formation is about 160 m thick. Three slightly different facies can be identified: a shaly facies in the lower half of the sequence, a 15 m thick sandy–limy facies in the middle of the sequence and a sandy facies interstratified with the shaly facies in the upper part (Thury and Bossart, 1999; Bossart et al., 2002). The shaly facies contains about 65% clay minerals and about 20% quartz. The sandy facies has a lower clay content of about 40% and a higher quartz component of about 30%. In the area where the rock laboratory is located, rock strata dip with an angle of approx-

Geological profile
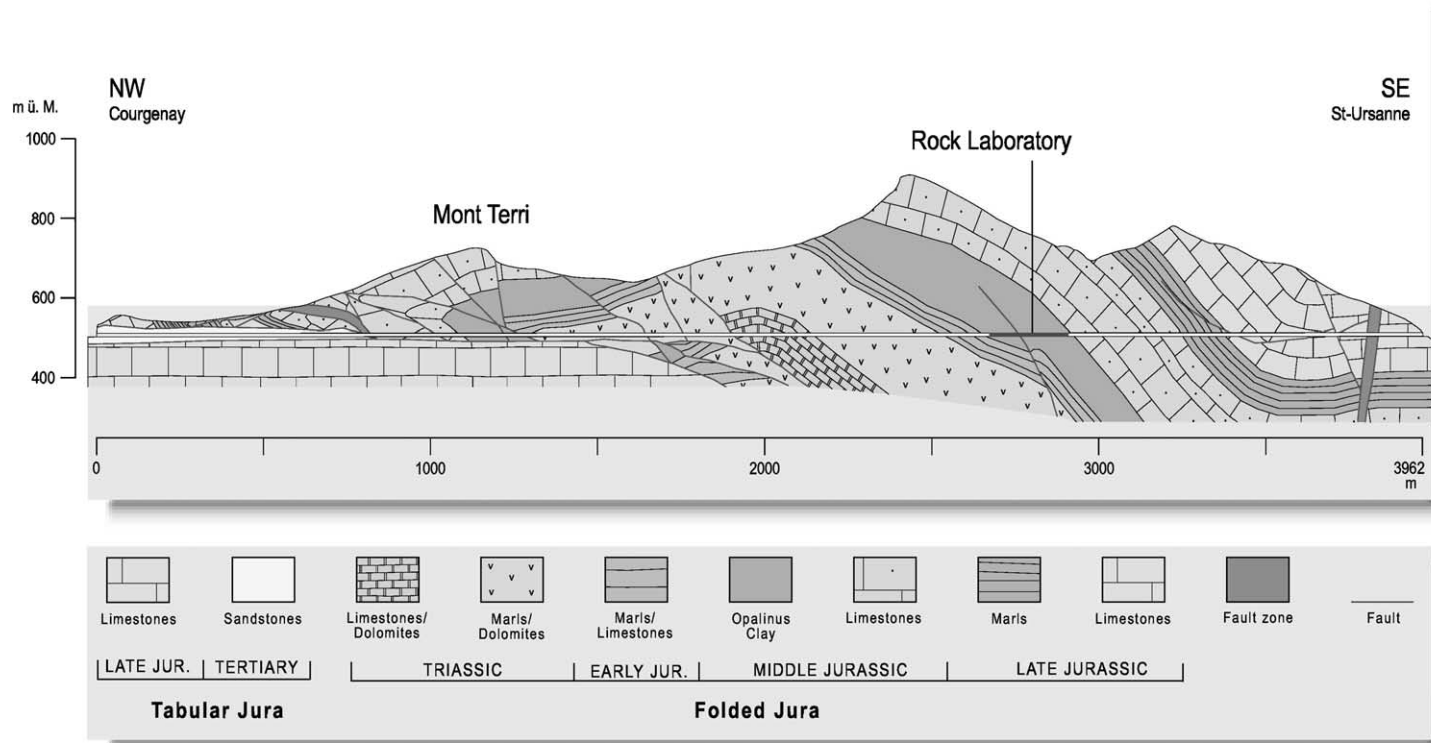## Balanced cross-section along Mont Terri motorway tunnel

Fig. 1. Geological vertical cross-section of the Mont Terri site (from http://www.mont-terri.ch).

imately 40° south-easterly and are penetrated by several minor faults. The opalinus clay has an extremely low hydraulic permeability, of the order of 2×10^{-13} m s^{-1}. The rock is finely porous and contains 4% to 12% water.

2.2. Equipment description

The main components of the experiment were a heating source with a heater power regulation unit and several temperature sensors with the required data acquisition and control components (see Fig. 2). The heating source was first put in a long steel tube and then set up in a 2.5 m deep vertical borehole (called BHE18) located close to the wall of the gallery. The borehole was then filled in with sand, buffer made up of bentonite, cement, sikadur 42 (a pourable epoxy grout) and epoxy resins. Some air was also present inside and above the tube containing the heating source. The borehole was closed up with a metallic cover. Temperature sensors were set up in the surrounding rock mass in two vertical boreholes of 36 mm in diameter and 2.5 m deep (see Fig. 3). These two boreholes, called BHE_C2 and BHE_C3, were drilled parallel to the BHE18 borehole and at a distance of about 0.5 m from it. Pt-100 sensors temperature probes were located 0.25 m apart from one another on two PVC tubes placed vertically in the BHE_C2 and BHE_C3 boreholes. The probes located in the BHE_C2 borehole are called BHE_C2-T1, BHE_C2-T2, BHE_C2-T3, BHE_C2-T4 and BHE_C2-T5. The probes located in the BHE_C3 borehole are called BHE_C3-T1, BHE_C3-T2, BHE_C3-T3, BHE_C3-T4 and BHE_C3-T5. A specific calibration of these Pt-100 sensors together with the data acquisition system was performed to obtain accurate temperature measurements (accuracy of about 0.1 °C). Thermocouples were also fixed to the heating element or put in the bentonite (see Fig. 3). The thermocouples fixed to the heating element are called THEB18_01.80, THEB18_01.80-PT/1, THEB18_01.95, THEB18_02.10 and THEB18_02.10-PT/2. The thermocouples placed in the bentonite are called TB18_01.70, TB18_01.90/1, TB18_01.90/2, TB18_01.90/3 and TB18_02.20. These thermocouples are less accurate than Pt-100 sensors (accuracy of about 1 °C). Heating began in borehole BHE18 on April 30th 2002.
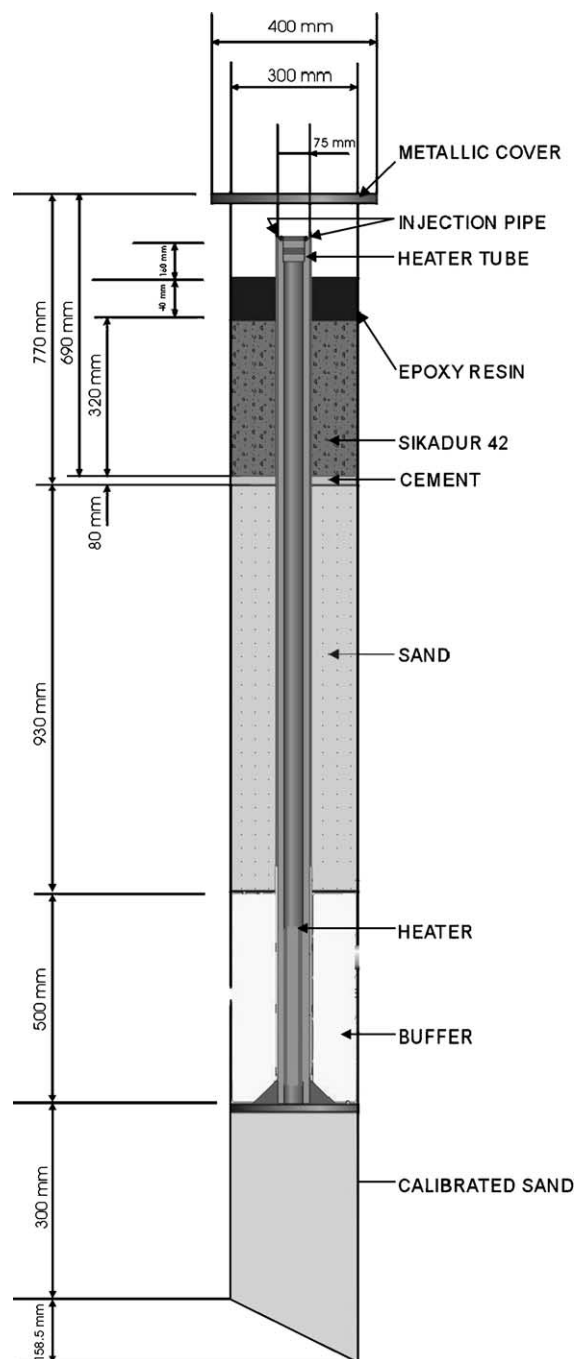

Fig. 2. Schematic vertical section of borehole BHE18 containing the heating source. The borehole is filled in with sand, buffer made up of bentonite, cement, sikadur 42 (a pourable epoxy grout) and epoxy resins. The borehole is closed up with a metallic cover.
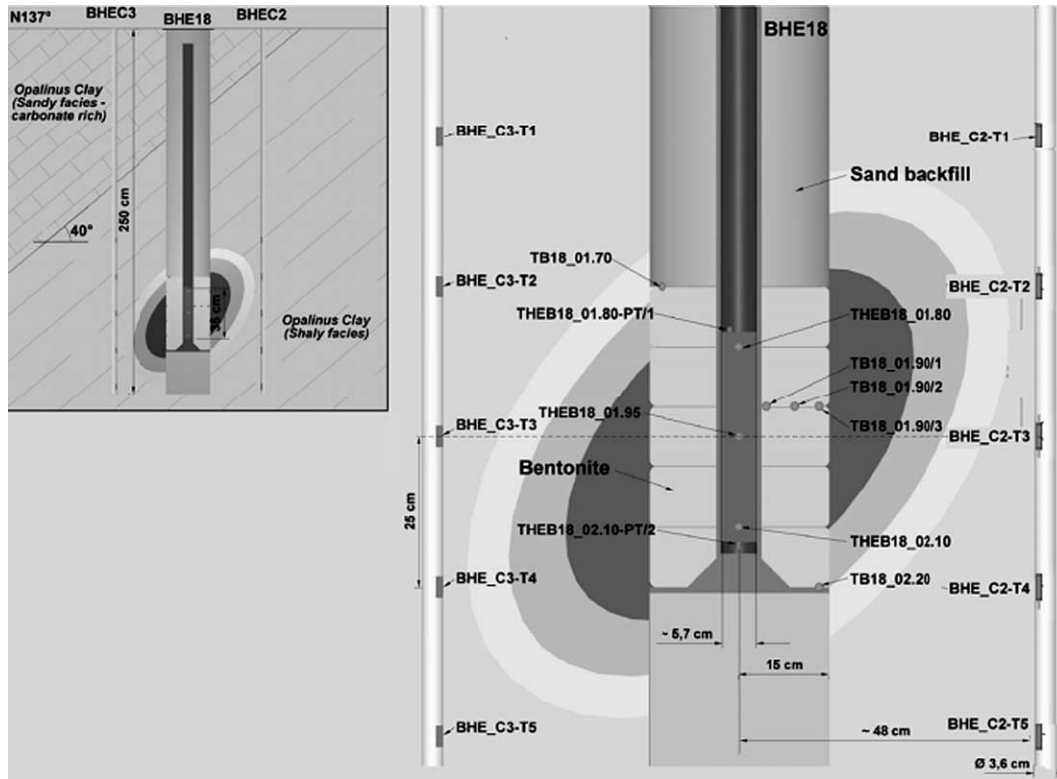
Fig. 3. Schematic vertical section of the laboratory at boreholes BHE18, BHE_C2 and BHE_C3. The heating source is centered in borehole BHE18. Boreholes BHE_C2 and BHE_C3 contain the temperature sensors. The 40° dip of the sedimentary layers can also be seen in the small panel and anisotropic thermal behaviour of the rock is schematized by ellipses whose major axis are parallel to the rock strata.

2.3. In-situ experimental results

Fig. 4 (a)–(d) show experimental measurements of the temperature versus time given by the probes located close to the heating source, in the bentonite, in the BHE_C2 borehole and in the BHE_C3 borehole, respectively. In the opalinus clay, the temperature rapidly increases during the first few days. Then, this increase slows down and the curves pass through a maximum after about 150 days of heating. The maximum temperatures lie between 20 and 30 °C depending on the position of the probe (see Fig. 4(c) and (d)). After 150 days, the temperature seems nearly constant; in actual fact, it slowly decreases by 0.5 to 1 °C over 100 days. This behaviour is closely connected with the temperature variation in the gallery located 2 m above the heating source (see Fig. 5). Indeed, the gallery is highly ventilated. As a consequence, the temperature in the gallery varies as the

season change. The continuous temperature decrease measured in the clay rock after 150 days occurred in autumn and winter. As it will be shown in next section, the gallery temperature fluctuations will have to be taken into account in the modelling.

As shown in Fig. 3, rock strata dip with an angle of approximately 40° south-easterly. This angle is close enough to a 45° angle to induce some kind of symmetry between the probes located in the BHE_C2 borehole and those located in the BHE_C3 borehole. Probes can be paired up as follows: BHE_C2-T1 and BHE_C3-T5, BHE_C2-T2 and BHE_C3-T4, BHE_C2-T3 and BHE_C3-T3, BHE_C2-T4 and BHE_C3-T2, BHE_C2-T5 and BHE_C3-T1 (see Fig. 3). However, Fig. 4(c) and (d) show that all temperatures experimentally measured in the BHE_C2 borehole are 1 to 3 °C higher than those measured in the BHE_C3 borehole. So, if we suppose that clay thermal properties are homogeneous, it seems difficult to obtain
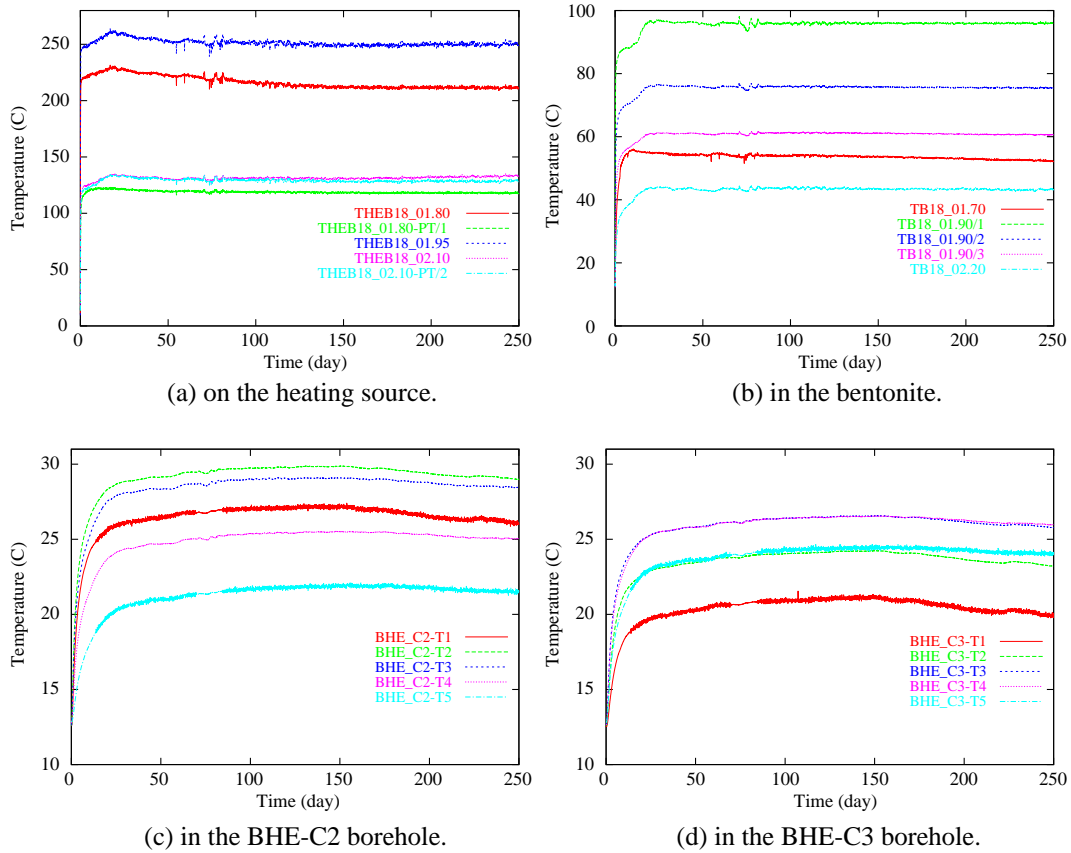
Fig. 4. Time evolution of the experimentally measured temperatures: (a) close to the heating source, (b) in the bentonite, (c) in the BHE_C2 borehole, (d) in the BHE_C3 borehole. (For interpretation of the references to colour in this figure legend, the reader is referred to the web version of this article.)

by simulation the difference observed during the experiment. The phenomenon observed might be explained by the presence of different thermal properties in the clay on either side of borehole BHE18, perhaps because of the presence of a bed of carbonated rock above probes BHE_C3 (see Fig. 3). The presence of fractures in the bentonite located around the heating source could also explain the lack of symmetry. This point will be taken into account during calculations to identify the thermal conductivity coefficients of the clay.

2.4. Experimental results obtained in laboratory

Experimental measurements of the thermal diffusivity have been performed in laboratory from four samples of argillite extracted from BHE_C2 and

BHE_C3 boreholes. These measurements have been performed in the LAEGO laboratory (Nancy, France) using the flash method (Schoumacker, 2003). The flash method is the most popular method used to measure the thermal diffusivity of materials (Parker et al., 1961). In this method, the front face of a small disk-shaped sample is subjected to a very short burst of radiant energy. The resulting temperature rise of the rear surface of the sample is measured and thermal diffusivity values are computed from the temperature rise versus time data. Samples are supposed isotropic and adiabatic. In experiments performed in the LAEGO laboratory, samples had a diameter comprised between 10 and 15 mm and a thickness of 7 to 8 mm. The source of the radiant energy was a flash lamp and irradiation times were less than 10 ms. Results are presented in Table 1.
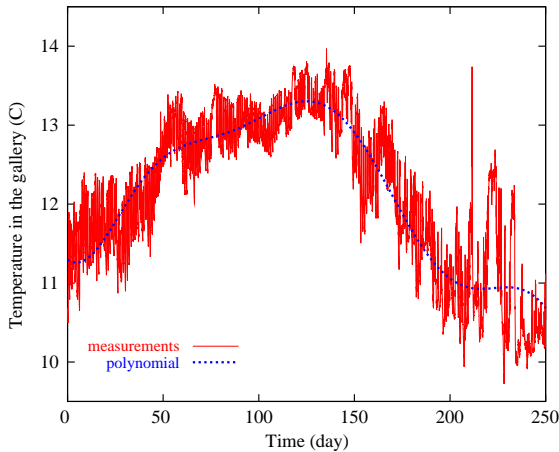
Fig. 5. Time evolution of the experimentally measured temperature in the gallery: experimental results and polynomial interpolation. (For interpretation of the references to colour in this figure legend, the reader is referred to the web version of this article.)

The accuracy is about 3%. Thermal conductivities λ are calculated from thermal diffusivities D according to the relation

$$\lambda = D\rho C_p, \tag{1}$$

where ρ and C_p are the heat capacity and bulk density of the argillite, respectively. The values of ρ and C_p for the opalinus clay are specified in Table 2. Table 1 shows that when thermal properties are assumed isotropic, measured thermal conductivities lie between 1.24 and 1.38 W m^{-1} K^{-1}. Other previous measurements of the thermal conductivity of the opalinus clay gave the following values (Nagra, 2001): $\lambda_{//}$=2.04 ± 0.23 W m^{-1} K^{-1} and $\lambda_{\perp}$=1.026 ± 0.11 W m^{-1} K^{-1}, where $\lambda_{//}$ and $\lambda_{\perp}$ are the thermal conductivities parallel and perpendicular to the bedding plane, respectively. It was also shown that, on one hand, the conductivity increases with the quartz content and, on the other hand, it

decreases of about 10% if the sample is desaturated. The decrease of thermal conductivity with desaturation was also measured on Callovian–Oxfordian argillite samples extracted from the site where ANDRA is building the French underground research laboratory (Homand, 1998).

3. Numerical modelling

3.1. Physical modelling of heat transfer

The principle of heat conservation gives the following equation for heat transfer in the porous medium made up of argillite (de Marsily, 1986)

$$\rho C_p \frac{\partial T}{\partial t} = \vec{\nabla} \cdot \left(\overline{\overline{\lambda}} \, \vec{\nabla} \, T \right) + Q, \tag{2}$$

with ρ the mass per unit volume (kg m^{-3}) and C_p the specific heat (J kg^{-1} K^{-1}) of the porous medium (water plus solid), T the temperature, Q the heating source term per unit volume (W m^{-3}), not zero only in the source zone where it is equal to the thermal power divided by the volume of the source, and $\overline{\overline{\lambda}}$ is the tensor of equivalent conductivity (W m^{-1} K^{-1}), which represents the conductivity of the porous medium in the absence of flow. As the clay rock in which the experiment is conducted is made up of sedimentary layers, the conductivity tensor $\overline{\overline{\lambda}}$ is orthotropic with components $\lambda_{//}$ and $\lambda_{\perp}$, in and perpendicular to the bedding plane, respectively.

3.2. Numerical modelling

3.2.1. Description of the numerical tool

All numerical simulations described in this paper are performed with the Cast3M code (Bernard-Michel et al., 2004), using a Petrov–Galerkin fi-

Table 1
Thermal diffusivities experimentally measured on samples by flash method (Schoumacker, 2003)

Borehole depth	Sample diameter (mm)	Sample thickness (mm)	Water content (%)	Thermal diffusivity (m^2 s^{-1})	Thermal conductivity (W m^{-1} K^{-1})
BHE-C2 1.3 m	10–15	7.24	2.86	6.65×10^{-7}	1.30
BHE-C2 2.6 m	10–15	8.54	2.79	6.34×10^{-7}	1.24
BHE-C3 2.1 m	10–15	8.63	1.56	7.05×10^{-7}	1.38
BHE-C3 2.8 m	10–15	7.84	1.70	6.59×10^{-7}	1.29

Table 2
Thermal properties (conductivity, specific heat) and density of various components of experiment HE-C

Component	Thermal conductivity λ (W m^{-1} K^{-1})	Specific heat C_p (J kg^{-1} K^{-1})	Density ρ (kg m^{-3})	References
Opalinus clay	$\lambda_{//}$ and $\lambda_{\perp}$	800	2450	
Mild steel tube	50	500	7860	(Tuñón, 2002)
Stainless steel heating component	16.3	502	8030	(Baumeister and Marks, 1967) p. 6–10
Bentonite (saturated)	1.28	1820	1540	(Tuñón, 2002)
Sand (saturated)	1.4	2030	1300	(Tuñón, 2002) for ρ and λ (Rohsenow and Hartnett, 1973) p. 2–70 for Cp
Epoxy resin (not charged)	0.2	1200	1200	(Bardonnet, 1992)
Sikadur 42	0.55	790	2000	http://www.sika.ch
Metal lid	81	452	7900	(Taine and Petit, 1995) p. 397
Air	0.03	1000	1	(Taine and Petit, 1995) p. 401

nite-element spatial scheme and a Crank–Nicholson's time discretization.

3.2.2. Mesh description

As already mentioned, the aim of the work presented in this paper is to quantify the heat transfer from the heating source to the surrounding clay. Consequently, the simulated domain is centered on borehole BHE18. Furthermore, the domain size has to be large enough to ensure that numerical results are not boundary conditions dependent. An extent of some 12 m on either side of the borehole was selected and proved necessary. As the heating source is located only 2 m below the surface and as measurements are taken over a period of several months, heat exchange at the top of the BHE18 borehole and at the top of the clay layer around it could not be simply modelled by a boundary condition. Furthermore, preliminary calculations showed the need not only to simulate the gallery and the surrounding rock, but also to consider seasonal temperature variations inside the gallery. No common symmetry could be found between geological characteristics of the natural site (geological layers with a 40° dip with respect to the horizontal) and geometric characteristics of the engineered structures (borehole BHE18 not centered in the gallery). So, 3 D simulations of the whole domain were necessary.

The complete 3 D mesh is done of 37 708 cells. It is refined only near the boreholes BHE18, BHE_C2 and BHE_C3. Mesh nodes are located at less than one millimetre from the experimental temperature probes position. The mesh was obtained from a preliminary spatial convergence study.

3.2.3. Heating source modelling

Heating began in borehole BHE18 on April 30th 2002. During the first days, the heating element was monitored by the heating power kept at 235 W. From May 17th 2002 to April 28th 2003, the heating was then monitored by keeping a constant temperature of 96 °C in the bentonite at probe TB18_01.90/1 (see Figs. 3 and 4 (b)). The idea is to model the behaviour of nuclear wastes that will be at a temperature slightly less than 100 °C (the water boiling temperature at the atmospheric pressure) when they will be put in the underground storage. Fig. 6 gives the time evolution of the experimentally measured thermal power that
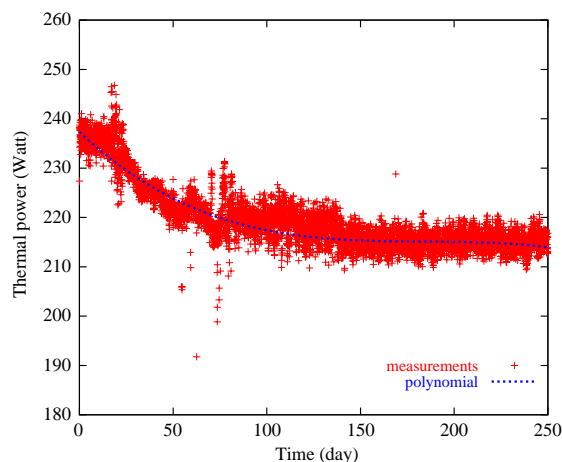

Fig. 6. Time evolution of the experimentally measured thermal power that supplies the heating source: experimental results and polynomial interpolation. (For interpretation of the references to colour in this figure legend, the reader is referred to the web version of this article.)

supplies the heating source. As can be seen in this figure, the mean thermal power decreases from 240 to 215 W during the first 150 days; afterwards, it is quite constant. This experimental time evolution was modelled by a polynomial of the 3rd degree (see Fig. 6). In theory, this thermal power divided by the source volume gives the Q term in Eq. (2) but in practice, this term has to be weighted by a multiplying factor noted α. This factor models heat losses between the power generator and the source, as well as all uncertainties of the thermal properties of various materials in borehole BHE18. The value of α will have to be determined by optimization together with the opalinus clay thermal conductivity coefficients.

3.2.4. Initial conditions

Eq. (2) must be solved in all engineered materials constituting the experiment set up of HE-C experiment (see Figs. 2 and 3) but also in the surrounding natural clay rock. Thermal characteristics of various materials (steel tube, heating source, engineered bentonite, sand,...) needed for the 3D direct simulation are given in Table 2. They are assumed independent of time. Indeed, laboratory measurements performed on argillite samples as similar as the Mont Terri rock showed that thermal conductivity of such an argillite slightly decreases with temperature (Giraud, 1995; Homand, 1998). But in the temperature range 20–80 °C, this decrease was of the order of magnitude of the precision (about 20%).

The initial temperature T_0 is supposed to be the same in the whole domain and equal to the mean value of the temperatures measured by the various probes at time $t = 0$: $T_0 = 12.75$ °C.

3.2.5. Boundary conditions

As the size of the simulated domain is large enough, homogeneous Neumann boundary conditions are imposed on all outer boundaries. However, on the gallery walls, heat exchanges are modelled using a convective boundary condition that gives the thermal flux through the gallery walls, Φ_{wall}, according to

$$\Phi_{wall} = h(T - T_{gallery}), \qquad (3)$$

where $T_{gallery}$ is the temperature in the gallery and h the transfer coefficient. Preliminary calculations showed the importance to take into account time

variations of the temperature $T_{gallery}$. Fig. 5 shows the measured time evolution of $T_{gallery}$ which can be modelled by a polynomial of the 10th degree. The coefficient h is assumed to be equal to the convective transfer coefficient in air, which lies between 5 and 30 W m^{-2} K^{-1} (Taine and Petit, 1995). Simulations were performed with the following value $h = 10$ W m^{-2} K^{-1}.

3.2.6. Time step

The time numerical scheme is a Crank–Nicholson's scheme. At the beginning of the experiment, when heating starts, heat transfer is highly unsteady and needs to be solved with accuracy. So, small time steps must be used. In the simulations presented in this paper, the first time step is equal to 1 s and gradually increases as follows: 10, 100, 1000, 10000 s. Then, it is constant and equal to half a day.

4. Optimization technique

4.1. Principle of the method

The longitudinal and transverse thermal conductivity values, respectively $\lambda_{//}$ and $\lambda_{\perp}$, and the heat dissipation coefficient α are determined using a numerical simulation–optimization technique. A standard least squares minimization technique should require about one hundred consecutive Cast3M direct simulations, with the risk to obtain only a local minimum of the objective function. So, we preferred to use a method allowing us to explore the entire parameter space. The various steps of this method are the following:

– step 1: the thermal model is solved for each value of the triplet $(\lambda_{//}, \lambda_{\perp}, \alpha)$ involved;
– step 2: an objective function that is the sum of the squared differences between measured and simulated temperatures is calculated;
– step 3: best values of triplet $(\lambda_{//}, \lambda_{\perp}, \alpha)$ are obtained by studying the isovalues of the objective function.

In step 1, a Cast3M direct numerical simulation should be done for each value of the triplet $(\lambda_{//}, \lambda_{\perp}, \alpha)$ involved. According to measurements performed in

laboratory, these values vary within the following ranges: $1 < \lambda_{//}$ (W m^{-1} K^{-1})< 4, $0.5 < \lambda_{\perp}$ (W m^{-1} K^{-1})< 3 and $0.7 < \alpha < 1$. So, the optimization technique requires thousands of Cast3M direct numerical simulations, each of which takes about 2.5 h CPU on Pentium IV. In order to drastically reduce the CPU time, the Cast3M code was approximated by a neural network.

4.2. Definition of the objective function

The objective function J is defined as follow

$$J = \sum_{i=1}^{ns} a_i (T\exp_i - T\mathrm{cal}_i)^2, \qquad (4)$$

with ns, the number of probes, a_i, a positive weighting coefficient with $\sum_i a_i = 1$, $T\exp_i$, the ith experimentally measured temperature, $T\mathrm{cal}_i$, the ith calculated temperature. Preliminary calculations showed that best results were obtained with all weighting coefficients equal to $1/ns$.

4.3. Choice of the temperature probes

Eleven temperature probes were used to calculate the objective function: the five probes located in the BHE_C2 borehole, the five probes located in the BHE_C3 borehole and the probe TB18_01.90/1 located in the bentonite near to the heating source (see Fig. 3). Temperature experimental measurements in opalinus clay have shown that there is no symmetry of the heat transfer with respect to the BHE18 borehole (see Fig. 4(c) and (d)). Therefore, the values of the thermal conductivities $\lambda_{//}$ and $\lambda_{\perp}$ were estimated separately on each side of the heating source, first by using the five probes located in the BHE_C2 borehole, second, by using the five probes located in the BHE_C3 borehole. In a third estimation, the probe TB18_01.90/1 located in the bentonite near to the heating source was also taken into account together with the five probes located in the BHE_C2 borehole. The α coefficient was supposed the same in all cases. Other calculations, not given in this paper, showed that it was useless to take into account the temperature results of the probe TB18_01.90/3. Furthermore, using the temperature results of the probes TB18_01.90/2 and TB18_01.70 gave bad results.

According to the time evolution of the temperature obtained from experimental measurements and preliminary Cast3M calculations, we assumed that a pseudo steady state was reached after 100 days in the opalinus clay where temperature probes are located, i.e., at about 0.5 m from the heating source. So, measured and simulated temperatures were averaged over the time interval [100, 150 days] and only these mean temperatures were used to calculate the objective function.

4.4. The neural network

The neural network approximation uses the NeMo CEA software (Dreyfus et al., 2002). It was built from a sample training of 1100 Cast3M direct simulations performed in parallel on several computers. The sampling of the parameters ($\lambda_{//}, \lambda_{\perp}, \alpha$) was done using the Latin Hypercube Sampling, a Design of Experiments method (Eldred et al., 2002) to explore the parameter space. A basic neural network was built for each of the temperature probes. We should have chosen to build only one neural network for all temperature probes but it would have been less accurate. The basic neural network includes one hidden layer made of 3 hidden neurones (see Fig. 7). Indeed, a simpler neural network with no hidden layer gave no satisfactory results. For each triplet ($\lambda_{//}, \lambda_{\perp}, \alpha$), the
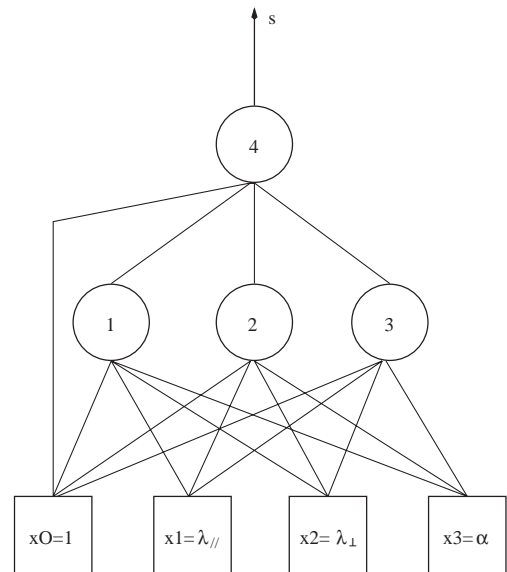

Fig. 7. Neural network with three hidden layers.

neural network calculates a temperature according to the following relation

$$S = \alpha_0 + \sum_{i=1}^{N\mathrm{hidden}} \alpha_i f \left(\sum_{j=1}^{N\mathrm{input}} w_{ij} x_j + w_{i0} \right), \qquad (5)$$

with S, the output variable (the calculated temperature at the considered probe), α_i and $w_{i,j}$, weights, Nhidden, the number of hidden neurons (3 in our case), x_j, the input parameter ($x_j = \lambda_{//}$, $\lambda_\perp$ or α), Ninput their number (3 in our case) and $f(x)$, the sigmoid activation function given by

$$f(x) = \frac{1}{1 + e^{-x}}. \qquad (6)$$

The global neural network is done of these various basic neural networks built for each of the temperature probes.

4.5. Optimization

The very fast neural network allowed us to approximate the Cast3M code and then to calculate the objective function given by Eq. (4) for 500 000 different values for the triplet ($\lambda_{//}, \lambda_\perp, \alpha$): 100 values of $\lambda_{//}$ in the range [1, 4], 100 values of $\lambda_\perp$ in the range [0.5, 3] and 50 values of α in the range [0.7, 1]. This number of 500 000 instantaneous calculations performed with the neural network has to be compared with the 1100 Cast3M preliminary direct simulations necessary to the neural network training. The best values of the triplet ($\lambda_{//}, \lambda_\perp, \alpha$) were obtained by solving the following inequality for the objective function

$$J < J_{\max} \qquad (7)$$

with J, the objective function given by Eq. (4). In this expression, $J_{\max}$ is the value of the objective function estimated by taking the maximum allowed values for ($T\mathrm{exp}_i - T\mathrm{cal}_i$) in the opalinus clay and in the bentonite, noted $\Delta T_{\max,\mathrm{opalinus}}$ and $\Delta T_{\max,\mathrm{bentonite}}$, respectively. As the accuracy of temperature measurements in opalinus clay and in the bentonite are equal to 0.1 and 1 °C, respectively, we will take $\Delta T_{\max,\mathrm{opalinus}} \geq 0.1$ °C and $\Delta T_{\max,\mathrm{bentonite}} \geq 1$ °C. A usual problem in optimization techniques is to obtain a local minimum of the objective function. With this method which calculates the objective function in a wide range of parameters ($\lambda_{//}, \lambda_\perp, \alpha$) and which con-

siders all solutions of Eq. (7), we are sure to obtain the real minimum of the function.

5. Results

As already mentioned, the values of the thermal conductivities $\lambda_{//}$ and $\lambda_\perp$ were estimated separately on each side of the heating source, first by using the five probes located in the BHE_C2 borehole (with or without the TB18_01.90/1 probe), second, by using the five probes located in the BHE_C3 borehole.

5.1. Using the BHE_C2 and TB18_01.90/1 probes

Several configurations were performed. First, the objective function was calculated with only the BHE_C2 probes. Its minimization was done according to Eq. (7) with two various values of $\Delta T_{\max,\mathrm{opalinus}}$: 0.25 and 0.5 °C. Second, the objective function was calculated with the BHE_C2 probes together with the TB18_01.90/1 probe. Its minimization was done according to Eq. (7) with the various following values of the pair ($\Delta T_{\max,\mathrm{opalinus}}$, $\Delta T_{\max,\mathrm{bentonite}}$): (0.10, 1 °C), (0.15, 1.5 °C), (0.25, 2.5 °C) and (0.50, 5 °C). Results are given in Fig. 8. Each symbol represents a pair ($\lambda_{//}, \alpha$) and ($\lambda_\perp, \alpha$) which satisfies the minimization criterion given by Eq. (7). This representation shows it is necessary to take into account the TB18_01.90/1 probe temperature in the calculation of the objective function. Indeed, without this probe, the value of α cannot be determined although the allowed value of α is in the range [0.74, 0.79] when this probe is taken into account. Finally, the ensemble of optimized values for the triplet ($\lambda_{//}, \lambda_\perp, \alpha$) is included in the intersection of the allowed values obtained from the various configurations. This domain is represented in yellow in Fig. 8 and is given by $\lambda_{//} = 1.84 \pm 0.04$ W m^{-1} K^{-1}, $\lambda_\perp = 0.55 \pm 0.03$ W m^{-1} K^{-1} and $\alpha = 0.77 \pm 0.03$.

5.2. Using the BHE_C3 probes

Similar calculations using the BHE_C3 probes were performed to determine the ($\lambda_{//}, \lambda_\perp, \alpha$) values on the other side of BHE18 borehole. In this case, the objective function was calculated with only the BHE_C3 probes. Its minimization was done according
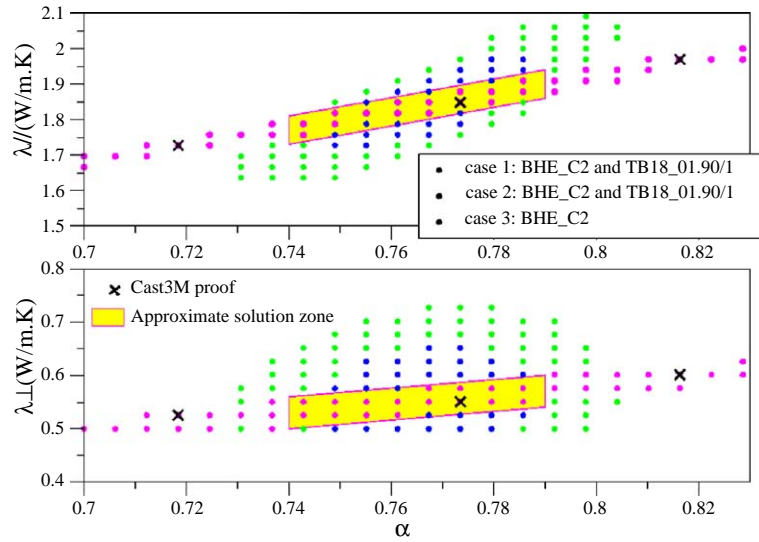
Fig. 8. Domain of optimized values for the triplet ($\lambda_{//}, \lambda_{\perp}, \alpha$) obtained from BHE_C2 probes with (cases 1 and 2) and without (case 3) the TB18_01.90/1 probe. Points correspond to triplets ($\lambda_{//}, \lambda_{\perp}, \alpha$) solutions of $J < J_{max}$ where J_{max} is calculated with ($\Delta T_{max,opalinus}$, $\Delta T_{max,bentonite}$) = (0.15, 1.5 °C) in case 1, ($\Delta T_{max,opalinus}$, $\Delta T_{max,bentonite}$) = (0.1, 1 °C) in case 2, and $\Delta T_{max,opalinus}$ = 0.25 °C in case 3. The yellow zones indicate the intersection of the optimized values obtained from these various cases. Black crosses indicate the values of the parameters chosen for three Cast3M direct simulations performed to validate the optimization technique. (For interpretation of the references to colour in this figure legend, the reader is referred to the web version of this article.)

to Eq. (7) with two various values of $\Delta T_{max,opalinus}$: 0.25 and 0.5 °C. As shown in Fig. 9, for all α values lying between 0.7 and 1, a triplet ($\lambda_{//}, \lambda_{\perp}, \alpha$) minimiz-

ing the objective function is available. Unfortunately, none of the probes next to the heating element could be used to stress the system. Indeed, several prelim-
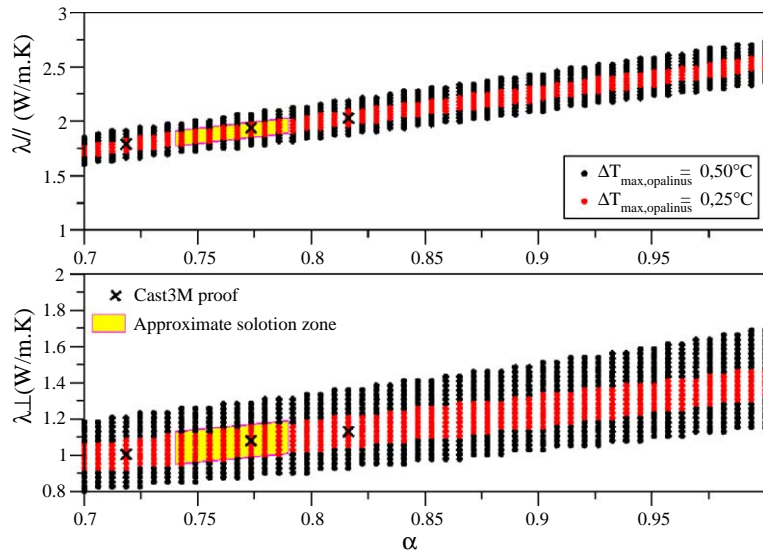

Fig. 9. Domain of optimized values for the triplet ($\lambda_{//}, \lambda_{\perp}, \alpha$) obtained from BHE_C3 probes. Black and red points correspond to triplets ($\lambda_{//}, \lambda_{\perp}, \alpha$) solutions of $J < J_{max}$ where J_{max} is calculated with $\Delta T_{max,opalinus}$ = 0.5 and 0.25 °C, respectively. (For interpretation of the references to colour in this figure legend, the reader is referred to the web version of this article.)

(a) t=1 day.

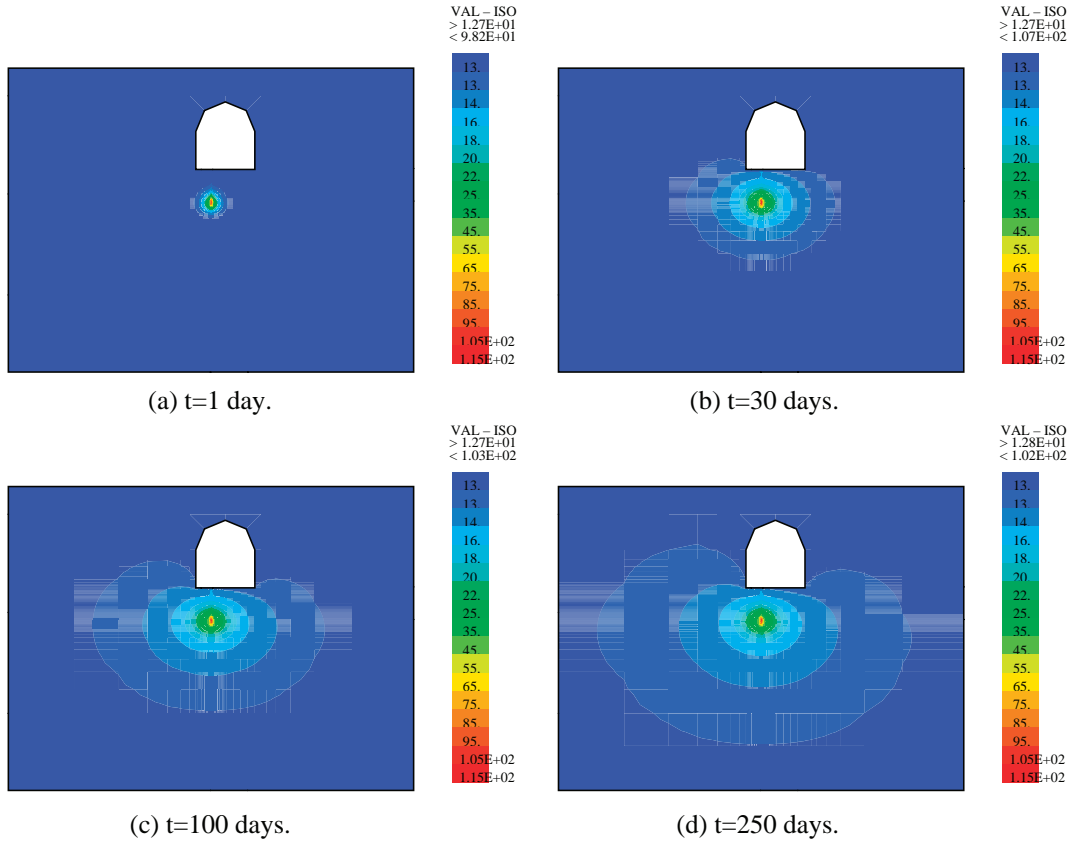(b) t=30 days.

(c) t=100 days.

(d) t=250 days.

Fig. 10. Cross-sections of the 3D temperature fields according to the vertical plane perpendicular to the gallery and passing through the vertical axis of symmetry of borehole BHE18, at four various times, (a) $t=1$ day, (b) 3 days, (c) 100 days and (d) 250 days. (For interpretation of the references to colour in this figure legend, the reader is referred to the web version of this article.)

inary calculations performed with these probes gave bad results: optimized values were obtained only for (Texp$_i$ − Tcal$_i$) greater than 0.8 °C. If we suppose that the factor α that models heat losses and uncertainties of the thermal properties of various materials in the BHE18 borehole is the same on each side of the borehole, we can take the values previously obtained, i.e., $\alpha \in [0.74, 0.79]$. The set of optimized values for the triplet ($\lambda_{//}, \lambda_\perp, \alpha$) is then represented in yellow in Fig. 9 and is given by $\lambda_{//} = 1.90 \pm 0.07$ W m^{-1} K^{-1}, $\lambda_\perp = 1.07 \pm 0.09$ W m^{-1} K^{-1} and $\alpha = 0.77 \pm 0.03$.

5.3. Discussion

The sets of optimized values for the triplet ($\lambda_{//}, \lambda_\perp, \alpha$) given previously have been obtained from optimization calculations based on a neural network. In order to check the validity of this method, some

direct numerical Cast3M simulations were performed with the three various following values of the triplet ($\lambda_{//}, \lambda_\perp, \alpha$): (1.727, 0.525, 0.718), (1.848, 0.550, 0.773) and (1.970, 0.601, 0.816) for BHE_C2 probes, (1.788, 1.005, 0.718), (1.939, 1.081, 0.773) and (2.030, 1.131, 0.816) for BHE_C3 probes. Fig. 10(a)–(d) give the cross-sections of the 3D temperature field at four various times, $t=1$, 30, 100 and 250 days, according to the vertical plane perpendicular to the gallery and passing through the vertical axis of symmetry of borehole BHE18. These figures, obtained with ($\lambda_{//}, \lambda_\perp, \alpha$)=(2.030, 1.131, 0.816), clearly show the expansion of the temperature disruption around the borehole and the gallery. After only 30 days, the disturbed zone extends on several metres around the heating source and has already reached the gallery's walls. After 250 days, the disturbed zone is still wider but the simulated domain is large enough to avoid

influences due to the external boundary conditions (see Fig. 10(d)). Fig. 11 displays the temperature evolutions versus time measured with the BHE_C2 and BHE_C3 probes and calculated with the six various triplets ($\lambda_{//}, \lambda_\perp, \alpha$). Experimental and numerical results are in good qualitative agreement. More quantitatively, for each probe i, we calculated the quantity ($T\exp_i - T\text{cal}_i$), where $T\exp_i$ and $T\text{cal}_i$ are the measured and simulated temperatures averaged over the time interval [100, 150 days]. As shown in Table 3, this quantity is always found less than 0.48 °C for the BHE_C2 probes. Less accurate results are obtained for the TB18_01.90/1 probe and only the triplet ($\lambda_{//}, \lambda_\perp, \alpha$)=(1.848, 0.550, 0.773) gives a difference between experimental and calculated temperatures less than 1 °C. Consequently, the lowest value for the objective function when the TB18_01.90/1 probe is taken into account is obtained with this triplet. On the other hand, as shown in Table 4, the quantity

($T\exp_i - T\text{cal}_i$) calculated from BHE_C3 probes is always less than 0.33 °C and the values obtained for the objective function are quite similar for the three different triplets ($\lambda_{//}, \lambda_\perp, \alpha$) involved.

Finally, these additional direct simulations prove that the neural network correctly simulates Cast3M calculations and that parameters ($\lambda_{//}, \lambda_\perp, \alpha$) obtained from optimization technique yield the correct measured temperatures. Furthermore, thermal conductivity mean values obtained from simulations of in situ experiments are of the same order of magnitude as those measured on samples by flash method (see Table 5). The longitudinal and transverse conductivities obtained from optimization of the temperatures measured in the BHE_C3 borehole are very close to the values measured on samples of opalinus clay with a 10% to 15% quartz content.

After about 1 year of in situ experimental temperature measurements, the thermal power for the heating
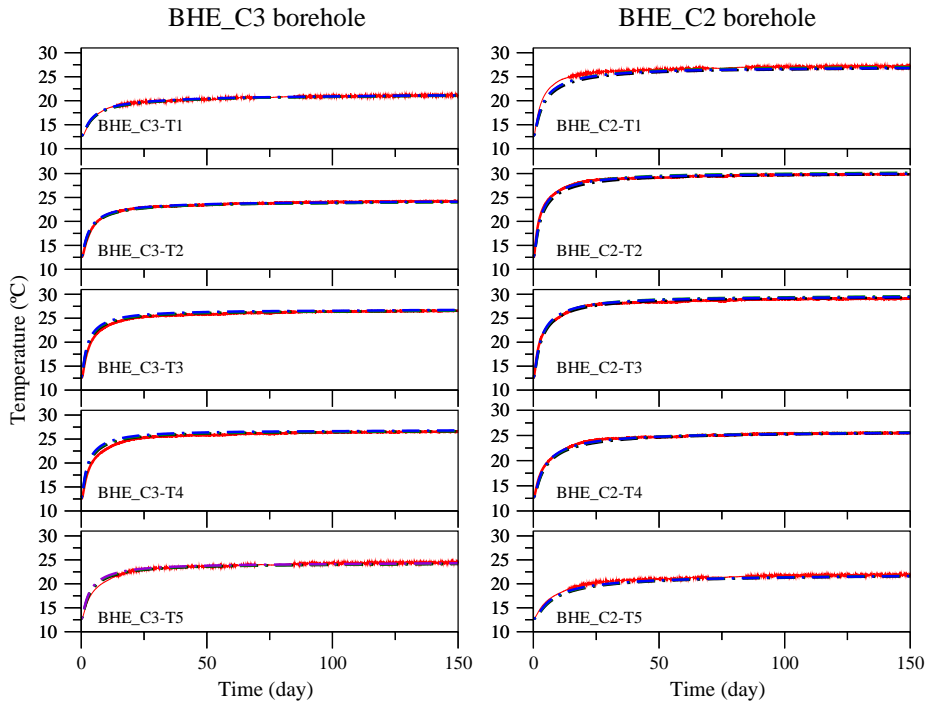

Fig. 11. Temperatures versus time obtained from experiments (red curves) and numerical simulations at the various probes located in BHE_C3 and BHE_C2 boreholes. Numerical simulations have been performed with several optimized values of $\lambda_{//}$, $\lambda_\perp$ (in W m^{-1} K^{-1}) and α. For the BHE_C3 borehole, the black, green and blue curves correspond to ($\lambda_{//}, \lambda_\perp, \alpha$)=(1.788, 1.005, 0.718), (1.939, 1.081, 0.773) and (2.030, 1.131, 0.816), respectively. For the BHE_C2 borehole, the black, green and blue curves correspond to ($\lambda_{//}, \lambda_\perp, \alpha$)=(1.727, 0.525, 0.718), (1.848, 0.550, 0.773) and (1.970, 0.601, 0.816), respectively. (For interpretation of the references to colour in this figure legend, the reader is referred to the web version of this article.)

Table 3
Difference between measured and simulated mean temperatures for BHE_C2 and TB18-01.90/1 probes

	$\lambda_{//}=1.727$ $\lambda_{\perp}=0.525$ $\alpha=0.718$	$\lambda_{//}=1.848$ $\lambda_{\perp}=0.550$ $\alpha=0.773$	$\lambda_{//}=1.970$ $\lambda_{\perp}=0.601$ $\alpha=0.816$
$(T_{exp}-T_{cal})$ for the following probes			
BHE_C2-T1	0.48	0.21	0.4
BHE_C2-T2	0.06	-0.27	-0.07
BHE_C2-T3	-0.17	-0.44	-0.29
BHE_C2-T4	0.11	-0.04	0.04
BHE_C2-T5	0.39	0.30	0.34
TB18-01.90/1	3.13	-0.69	-2.84
Objective function J			
Calculated from the five BHE_C2 probes	0.085	0.080	0.073
Calculated from the five BHE_C2 probes and from the TB18-01.90/1 probe	1.704	0.146	1.405

The objective function J is calculated from the five BHE_C2 probes and with or without the TB18-01.90/1 probe.

element was decreased and kept equal to 92 W. Cast3M direct numerical simulations were then performed with the thermal conductivity values previously determined, i.e., $\lambda_{//}=1.84$ W m^{-1} K^{-1} and $\lambda_{\perp}=0.55$ W m^{-1} K^{-1} on one side of the heating source (BHE_C2 borehole) and $\lambda_{//}=1.90$ W m^{-1} K^{-1} and $\lambda_{\perp}=1.07$ W m^{-1} K^{-1} on the other side (BHE_C3 borehole). On the other hand, the weighting coefficient α was not the same before and after the power decrease: its value was first equal to 0.77 and, after the power decrease, it was equal to 0.9. The fact that the percentage of thermal losses increase with the injected electric power is not so surprising. Fig. 12 gives the comparison between experimental and calculated temperatures in the opalinus clay. Measurements and simulations ended on June 30th 2003. As shown in Fig. 12, experimental and numerical temperature evolutions in the opalinus clay are in quite good agreement. It proves that the values obtained for $\lambda_{//}$ and $\lambda_{\perp}$ are still valid.

6. Conclusion

In this paper, we have presented experiments and calculations performed to determine the thermal conductivity of the opalinus clay in the Mont Terri underground laboratory. The experiment, called HE-C, consisted in measuring in situ clay temperature variation when submitted to a heating source. Experimental measurements were then used to determine the thermal conductivity via an optimization technique.

Experimental temperature study and preliminary direct numerical simulations of the HE-C experiment revealed the following several points. First, 3D simulations were required because of the lack of common symmetry between geological characteristics of the natural site and geometric characteristics of the engineered structures. Secondly, the seasonal variation of the temperature in the gallery located about 2 m above the heating source had to be taken into account. Thirdly, there was no symmetry between the thermal behaviour observed on either side of the BHE18 borehole containing the heating source. So, the thermal conductivity values of opalinus clay on either side of the heating source had to be determined separately. Fourthly, the heating source had to be weighted by a multiplying factor α modelling the heat dissipation.

An optimization technique was used to identify the longitudinal $\lambda_{//}$ and transverse $\lambda_{\perp}$ thermal conductivities of the opalinus clay. It consists in calculating and studying an objective function that is the sum of the squared differences between measured and calculated temperatures. But this method induced a lot of Cast3M simulations. In order to drastically reduce the CPU time, we used a neural network approximation built from a sample training

Table 4
Difference between measured and simulated mean temperatures for the BHE_C3 probes

	$\lambda_{//}=1.788$ $\lambda_{\perp}=1.005$ $\alpha=0.718$	$\lambda_{//}=1.939$ $\lambda_{\perp}=1.081$ $\alpha=0.773$	$\lambda_{//}=2.030$ $\lambda_{\perp}=1.131$ $\alpha=0.816$
$(T_{exp}-T_{cal})$ for the following probes			
BHE_C3-T1	0.07	0.10	0.02
BHE_C3-T2	0.20	0.22	0.10
BHE_C3-T3	-0.01	-0.01	-0.17
BHE_C3-T4	-0.06	-0.09	-0.25
BHE_C3-T5	0.33	0.31	0.18
Objective function J			
Calculated from the five BHE_C3 probes	0.032	0.033	0.027

The objective function J is calculated from the five BHE_C3 probes.

Table 5
Comparison of the values of the thermal conductivity measured on samples with the values obtained from the numerical simulation–optimization technique

		$\lambda_{//}$ (W m^{-1} K^{-1})	$\lambda_{\perp}$ (W m^{-1} K^{-1})	$(\lambda_{//}+\lambda_{\perp})/2$ (W m^{-1} K^{-1})
Simulation–optimization technique	BHE_C2	1.84 ± 0.04	0.55 ± 0.03	1.20
	BHE_C3	1.90 ± 0.07	1.07 ± 0.09	1.49
Measurements (Nagra, 2001)	Opalinus clay (10–15% content quartz)	2.04 ± 0.23	1.26 ± 0.11	1.65
Measurements (Schoumacker, 2003)	BHE_C2			1.27
	BHE_C3			1.33

of 1100 Cast3M simulations. It allowed us to calculate the objective function for 500 000 different values of the triplet ($\lambda_{//}$,$\lambda_{\perp}$,α). Finally, we obtained the following values for the thermal conductivities

– on one side of the heating source (BHE_C2 borehole): $\lambda_{//}$=1.84 ± 0.04 W m^{-1} K^{-1} and $\lambda_{\perp}$=0.55 ± 0.03 W m^{-1} K^{-1};

– on the other side of the heating source (BHE_C3 borehole): $\lambda_{//}$=1.90 ± 0.07 W m^{-1} K^{-1} and $\lambda_{\perp}$=1.07 ± 0.09 W m^{-1} K^{-1}.

It can be seen that the longitudinal conductivity $\lambda_{//}$ is quite homogeneous throughout the domain and very close to values measured on samples in laboratory. Transverse conductivity values, however, vary by a
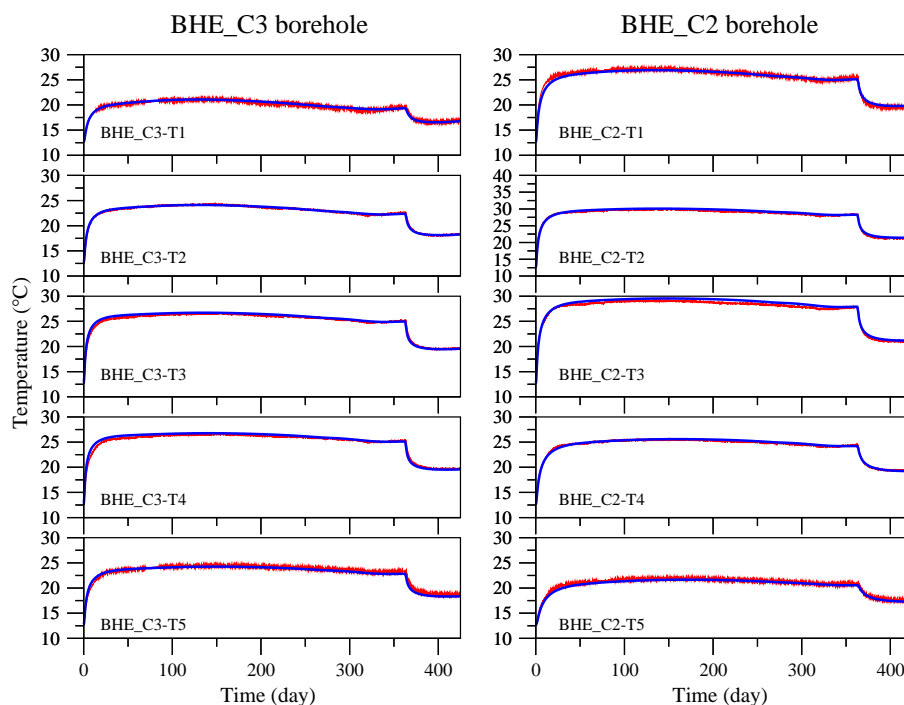

Fig. 12. Temperatures versus time obtained from experiments (red curves) and numerical simulations at the various probes located in BHE_C3 and BHE_C2 boreholes, before and after the heating power decrease. For the BHE_C3 borehole, the numerical simulation has been performed with $\lambda_{//}$=1.9 W m^{-1} K^{-1} and $\lambda_{\perp}$=1.07 W m^{-1} K^{-1}. For the BHE_C2 borehole, the numerical simulation has been performed with $\lambda_{//}$=1.84 W m^{-1} K^{-1} and $\lambda_{\perp}$=0.55 W m^{-1} K^{-1}. In both cases, α=0.77 and 0.9 before and after the heating power decrease, respectively. (For interpretation of the references to colour in this figure legend, the reader is referred to the web version of this article.)

factor of 2. It is probably due to the presence of an intensive fractured zone on one side of the borehole, caused by bentonite swelling and involving local rock desaturation but it can also be due to the presence of a bed of carbonated rock. Measurements on sample showed that the thermal conductivity decreases if the sample is desaturated or if its quartz content decreases. Using probes located in the bentonite near the heating source together with the BHE_C3 probes might have allowed us to optimize α and perhaps to obtain thermal conductivities not so different on either side of the heating element. The heat dissipation coefficient α was found equal to 0.77 ± 0.03 but its value depends on the electric power injected in the heating source.

The study highlighted the importance of instrumentation location. The accuracy of the optimization method requires to measure the temperature at several points located in boreholes parallel to the heating source (here, BHE_C2 and BHE_C3 boreholes) but measurements on an axis perpendicular to this common direction is also required (here, probe TB18_01.90/1). Finally, in this paper, we showed the interest of numerical simulation–optimization technique coupled with neural network to determine rock properties that are difficult to be directly measured in situ.

References

Andra, 2003. Understanding deep geological disposal, Publication de l'Agence Nationale pour la gestion des Déchets Radioactifs, Références Séries.

Bardonnet, P., 1992. Résines époxydes: composants et propriétés. Techniques de l'Ingénieur A3 (465), 1–16.

Baumeister, T., Marks, L.S., 1967. Standard Handbook for Mechanical Engineers, Seventh edition. McGraw Hill.

Bernard-Michel, G., Le Potier, C., Beccantini, A., Gounand, S., Chraibi, M., 2004. The Andra couplex 1 test case: comparisons between finite-element, mixed hybrid finite element and finite volume discretizations: simulations of transport around a nuclear waste disposal site. Computational Geosciences 8, 187–201.

Bossart, P., Meier, P.M., Möri, A., Trick, Th., Mayor, J.-C., 2002. Geological and Hydraulic Characterization of the Excavation Disturbed Zone in the Opalinus Clay of the Mont Terri Rock Laboratory, Engineering Geology, vol. 66. Elsevier.

Croisé, J., Schlickenrieder, L., Marschall, P., Boisson, J.Y., Vogel, P., Yamamoto, S., 2004. Hydrogeological investigations in a low permeability claystone formation: the Mont Terri rock laboratory. Physics and Chemistry of the Earth 29, 3–15.

de Marsily, G., 1986. Quantitative Hydrogeology. Academic Press Inc. (London), Harcourt Brace Jovanovich Publishers.

Dreyfus, G., Martinez, J.-M., Samuelides, M., Gordon, M.B., Bardan, F., Hérault, L., 2002. Réseaux de neurones, méthodologie et applications. Eyrolles.

Eldred M.S., Giunta A.A., van Bloemen Waanders B.G., Wojtkiewicz S.F., Hart W.E., Alleva M.P., 2002. DAKOTA, a multilevel parallel object-oriented framework for design optimization, parameter estimation, uncertainty quantification, and sensitivity analysis. Version 3.0 Users' manual, tech. Rep. SAND2001-3796, Sandia National Laboratories, http://endo.sandia.gov/DAKOTA/.

Gautschi, A., 2001. Hydrogeology of a fractured shale (opalinus clay): implications for deep geological disposal of radioactive wastes. Hydrogeology Journal 9, 97–107.

GeoProc, 2003. Proceedings of the International Conference on Coupled T–H–M–C processes in Geo-systems: Fundamentals, Modelling, Experiments and Applications 13–15 October 2003, Stockholm, Sweden.

Giraud H., 1995. Mesure des paramètres thermiques et des caractéristiques thermomécaniques des marnes du Callovo–Oxfordien de la Haute-Marne. Technical Report ANDRA n°B RP 0ENG 95-009/A.

Homand F., 1998. Mesures thermiques sur le site Est, Technical Report ANDRA n°B RP 0ENG 98-009/A.

Lalieux, P., Thury, M., Horsman, S., 1996. Radioactive waste disposal in Argillaceous media. Newsletter, vol. 34. OCDE/NEA.

Nagra, 2001. Sondierbohrung Benken-Untersuchungsbericht. Nagra Internal Report NTB 00-01.

Nagra, 2002. The Mont Terri rock laboratory. Nagra Bulletin 34.

Parker, W.J., Jenkins, W.J., Butler, C.P., Abbott, G.L., 1961. Flash method of determining thermal diffusivity, heat capacity and thermal conductivity. Journal of Applied Physics 32.

Rohsenow, W.M., Hartnett, J.P., 1973. Handbook of Heat Transfer. Mc Graw Hill.

Schoumacker, L., 2003. HE-C experiment, Thermal Diffusivity Measurements on Opalinus Clay using Flash Method, Mont Terri Project Technical Note 2003-38.

Stephansson, O., Jing, L., Tsang, C.-F., 1996. Coupled Thermo–Hydro–Mechanical Processes of Fractured Media-Mathematical and Experimental Studies, Development in Geotechnical Engineering, vol. 79. Elsevier, Amsterdam.

Taine, J., Petit, J.-P., 1995. Cours et données de base, Transferts thermiques, Mécanique des fluides anisotropes. Dunod.

Thury, M., Bossart, P., 1999. The Mont Terri rock laboratory, a new international research project in a Mesozoic shale formation, in Switzerland. Engineering Geology 52, 347–359.

Tuñón S., 2002 (Private Communication).